

Enhanced Collisional Losses from a Magnetic Mirror Using the Lenard-Bernstein Collision Operator

Maxwell H. Rosen^{1†}, W. Sengupta¹, I. Ochs¹, F. I. Parra^{1,2},
and G. W. Hammett²

¹Department of Astrophysical Sciences, Princeton University, Princeton, NJ 08540, USA

²Princeton Plasma Physics Laboratory, Princeton, NJ 08540, USA

(Received xx; revised xx; accepted xx)

Collisions play a crucial role in governing particle and energy transport in plasmas confined in a magnetic mirror trap. Modern gyrokinetic codes are used to model transport in magnetic mirrors, but some of these codes utilize approximate model collision operators. This study focuses on a Pastukhov-style method of images calculation of particle and energy confinement times using a Lenard-Bernstein model collision operator. Prior work on parallel particle and energy balances used a different Fokker-Planck plasma collision operator and the method needs to be extended in non-trivial ways to study the Lenard-Bernstein operator. To assess the effectiveness of our approach, we compare our results with a modern finite element solver. Our findings reveal that the particle confinement time scales like $a \exp(a^2)$ using the Lenard-Bernstein operator, in contrast to the more accurate scaling that the Coulomb collision operator would yield $a^2 \exp(a^2)$, where a^2 is approximately proportional to the ambipolar potential. We propose that codes modeling collisional losses in a magnetic mirrors utilizing the Lenard-Bernstein or Dougherty collision operator scale their collision frequency of any electrostatically confined species. This study illuminates the intricate role the collision operator plays in the Pastukhov-style method of images calculation of collisional confinement.

1. Introduction

Magnetic mirrors, or adiabatic traps, present a compelling avenue for plasma confinement through the deflection of particles away from high-field regions. In recent years, the resurgence of interest in mirrors as a fusion concept has been led by groundbreaking experiments at the collisional Gas Dynamic Trap Experiment (GDT) at the Budker Institute in Novosibirsk, Russia, which achieved unprecedented transient electron temperatures of 900 eV, demonstrating the viability of mirrors in fusion endeavors (Bagryansky *et al.* 2015).

One of the most remarkable results from the GDT experiment is the stabilization of axisymmetric mirrors against the well-understood interchange instability (Post & Rosenbluth 1966). Vortex confinement, for instance, has been shown to stabilize the $m = 1$ flute interchange mode, and finite Larmor radius effects can stabilize $m \geq 2$ (Beklemishev *et al.* 2010; Bagryansky *et al.* 2011; Beklemishev 2017; Ryutov *et al.* 2011; White *et al.* 2018). Moreover, recent advancements in superconducting magnet technology and electron cyclotron heating (ECH) have motivated new experiments to extend the results of GDT (Fowler *et al.* 2017). One such experiment is the Wisconsin high-field

† Email address for correspondence: mhrosen@pppl.gov

axisymmetric mirror experiment (WHAM) in Madison, Wisconsin (Egedal *et al.* 2022; Endrizzi *et al.* 2023). Their new endeavor, utilizing high-temperature superconducting (HTS) REBCO tapes and neutral beam injection (NBI), will investigate the magneto-hydrodynamic (MHD) and kinetic stability of the axisymmetric mirror, extended into the collisionless regime. With these new experimental techniques and MHD stability in sight, questions arise related to particle and energy confinement in these new stable axisymmetric mirror configurations.

Parallel losses play a critical role in the confinement of particles and energy, which occur when particles scatter due to collisions across the loss cone (Berk & Chen 1988). Pastukhov (1974) laid the foundation for calculating parallel losses in a magnetic mirror with the method of images approach that this study utilizes. Pastukhov’s insight showed that the steady-state balance between a low-energy source, Fokker-Planck collision operator, and high-energy image sinks could be simplified by transforming the problem into an analogous Poisson equation, then solved using standard techniques from electromagnetism (Jackson 1999). Building on Pastukhov’s insight, Najmabadi *et al.* (1984) extended the analysis by simplifying Pastukhov’s variable transformations, reducing the number of approximations made, and including a higher-order correction, yielding a more refined solution. Recent advancements have been made by Ochs *et al.* (2023), who included relativistic effects to Najmabadi’s approach.

Although parallel dynamics are often the fastest time-scale phenomenon in magnetized plasmas, many researchers are interested in studying the next-order perpendicular transport due to micro-stability and turbulence, which find their best answers in computer simulations that include collisions. With the recent investigations using the Gkeyll code to study high-field magnetic mirrors utilizing the Dougherty collision operator (Francisquez *et al.* 2023), it is essential to understand the effect of this approximate collision operator on parallel collisional losses before it is extended to study perpendicular transport.

To understand the key details and trade-offs between different collision operators, we must first study a few important approximations in this context. A comprehensive description of two-particle collisions within the framework of a Fokker-Planck operator involves the so-called ‘Rosenbluth potentials’ (Rosenbluth *et al.* 1957). This full-fledged operator, while widely studied and implemented, poses computational and analytical challenges (Taitano *et al.* 2015). In some cases, approximations become a pragmatic necessity to render the problem computationally tractable. In this context, one widely used approximate collision operator is the Lenard-Bernstein (LBO) / Dougherty operator: a simple operator that captures the advection and diffusion responses from small-angle two-body collisions (Lenard & Bernstein 1958; Dougherty 1964). The difference between the LBO and Dougherty collision operators is that the LBO has zero parallel streaming fluid flow velocity, while the Dougherty operator includes the parallel fluid flow velocity in calculating the drag.

Novel work was performed using the Gkeyll code in projecting the Dougherty operator onto a discontinuous Galerkin framework with enhanced multi-species collisions for gyrokinetic and Vlasov-Maxwell simulations (Hakim *et al.* 2020; Francisquez *et al.* 2020, 2022). Owing to the Dougherty operator having eigenfunctions of Hermite polynomials, the GX code uses this simple collision operator (Mandell *et al.* 2022). The GENE-X code can simulate x-point geometry tokamak configurations, with their most rigorous collision operator being Dougherty (Ulbl *et al.* 2022, 2023). Other examples of plasma kinetic/gyrokinetic codes that have implemented such collision operators (at least as an option) include: Ye *et al.* (2024), Celebre *et al.* (2023), Hoffmann *et al.* (2023), Frei *et al.* (2022), Perrone *et al.* (2020), Loureiro *et al.* (2016), Grandgirard *et al.* (2016), Pezzi *et al.* (2016), Parker & Dellar (2015), and Hatch *et al.* (2013). An LBO / Dougherty

collision operator with the appropriate definitions satisfies many properties of a good collision operator, such as conservation of density, momentum, and energy (Francisquez *et al.* 2020). The most significant defect in this model is that the collision frequency is independent of velocity, leading to inaccurate results in the tail of the distribution function. Furthermore, the operator's isotropic diffusion coefficient makes no distinction between pitch-angle scattering and energy diffusion (Hirshman & Sigmar 1976). Some of the shortcomings of the Lenard-Bernstein/Dougherty operator are described in Knyazev *et al.* (2023).

In this study, we build upon the method of images approach developed by Najmabadi *et al.* (1984), but with a focus on the LBO, since we consider a system with zero parallel fluid flow. Since the ambipolar potential of magnetic mirrors shifts the loss cone towards higher-energy particles, we must investigate the validity of the LBO's collisionality approximation at high energies. Following the method of images approach from Najmabadi *et al.* (1984), results show that the particle confinement time scales like $a \exp(a^2)$ using the LBO, in contrast to the scaling $a^2 \exp(a^2)$ that more accurate Coulomb collision operator yields, where a^2 is proportional to the ambipolar potential. In addition, the average energy of lost particles is also modified. The error between the average energy of lost particles and our numerical solver is comparable to the study of Najmabadi *et al.* (1984). It is critical that a code utilizing the LBO or Dougherty collision operator matches particle loss rates compared to an experiment to predict the correct ambipolar potential. Suggestions are made to reduce the collision frequency to match particle loss rates compared to the results in Najmabadi *et al.* (1984).

It is of interest to mention and discuss an alternative to the method of images approach, as the historical journey toward accurate ambipolar estimates encompasses diverse approaches. Chernin & Rosenbluth (1978) introduced an alternative derivation that approximates the loss cone as a square in velocity space, yielding insights using a linearized Fokker-Planck equation and the associated variational principle. Cohen *et al.* (1978) showed that Chernin & Rosenbluth (1978) techniques lacked robustness compared to Pastukhov's technique, and higher-order approximations were needed. Subsequent work in Catto & Bernstein (1981), followed by Catto & Li (1985) and Fyfe *et al.* (1981), refined this approach by eliminating the square loss cone approximation and extending the approach to higher order. Catto's studies circumvent the need for an accurate solution for the distribution function by transforming the problem into parallel and perpendicular coordinates to the loss cone and then employing variational techniques to yield improved confinement times. Khudik (1997) demonstrated the comparable accuracy of fourth-order extensions of Catto's methods to Najmabadi's approach. Furthermore, these variational methods generalize to arbitrary mirror ratios and, therefore, would be more suitable for application to toroidal confinement devices, which have order unity mirror ratios. Extending these models to the LBO would not be trivial because these methods are finely tuned to the Coulomb operator. Although these methods have many good properties, we are ultimately interested in large mirror ratios, and the flexibility of variational techniques is unnecessary.

Subsequent sections will use the method of images approach to explore how the LBO collision operator changes the parallel losses of a magnetic mirror. In section 2, the problem is presented and solved systematically for the confinement time and energy loss rate. A correction factor is evaluated numerically in section 3. Results are compared to the numerical model presented in section 3. This approach's validity and applicability to mirror simulation codes are discussed in section 4. Suggestions are made for modifying the collision frequency to obtain the appropriate ambipolar potential. Finally, we conclude in section 5.

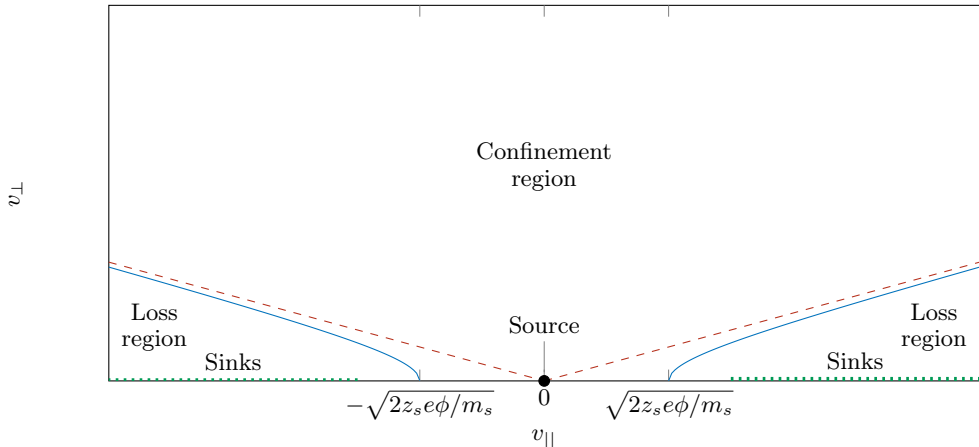


FIGURE 1. The loss boundary in velocity space for electrostatically confined particles in a magnetic mirror field. Imposed on the figure is a model depiction of the low energy source. The dotted green line represents the sinks used to solve for the distribution function. The blue line is the loss hyperboloid described in equation (2.1), and the red dashed line is the loss cone without an ambipolar potential.

2. Method of Images Solution

In a single-particle picture of a magnetic mirror, the parallel dynamics of particle losses depend on whether they possess sufficient energy to overcome the confining forces. These forces arise from gradients in the magnetic field magnitude ($\vec{\nabla}B$) and an electrostatic ambipolar potential ($z_s e \phi$), where e is the elementary charge and z_s is the charge number of species s . When particles have enough energy to overcome the $\vec{\nabla}B$ forces in the absence of an ambipolar potential, they reside within a specific region in phase space known as the “loss cone.” The introduction of an ambipolar potential alters the minimum energy required for escape, thereby transforming the loss cone into a “loss hyperboloid.” We parameterize the loss hyperboloid as follows.

$$1 - \mu^2 = \frac{1}{R} \left(1 - \frac{v_0^2}{v^2} \right). \quad (2.1)$$

Here, $\mu = \cos \theta = v_{\parallel}/v$ is the cosine of the pitch angle, v is the total velocity $|\vec{v}|$, $v_{\parallel} = (\vec{v} \cdot \vec{B})/B$ is the component of the velocity parallel to the magnetic field, R is the ratio of the maximum magnetic field to the minimum magnetic field B_{\max}/B_{\min} , and v_0 is the loss velocity corresponding to the ambipolar potential ($m_s v_0^2/2 = z_s e \phi$), where m_s is mass. The goal is to recreate this boundary, where the distribution function is null, with image sources and sinks. A model of the loss hyperboloid, source, and image sinks in the problem is shown in figure 1. A source is placed at a low velocity, in a steady state balance with the collision operator, while sinks are placed in the loss region and f_s is extended. With these sinks, the equation for f_s near the loss hyperboloid is

$$\mathcal{L}(f_s) + Q(v, \mu) = 0. \quad (2.2)$$

Here, $\mathcal{L}(f_s)$ is a collision operator which acts on the distribution function f_s of species s , and $Q(v, \mu)$ is an image sink of particles placed inside the loss region, where f_s is extended. The sink Q will be chosen to make $f_s = 0$ at the loss hyperboloid’s vertex defined by equation (2.1) as well as have the contour of $f_s = 0$ match the radii of

curvature of the loss hyperboloid at the vertex. Thus the boundary conditions on f_s are defined as

$$f_s(v, \mu)|_{v=v_0, \mu=\pm 1} = 0, \quad \left. \frac{\partial_v f_s}{\partial_\mu f_s} \right|_{v=v_0, \mu=\pm 1} = \frac{1}{Rv_0}. \quad (2.3)$$

For small v , we assume that f_s is a Maxwellian,

$$f_s(v, \mu)|_{v \rightarrow 0} \rightarrow \frac{n_s}{\pi^{3/2} v_{th,s}^2} \exp\left(-\frac{v^2}{v_{th,s}^2}\right), \quad (2.4)$$

where n_s is number density, $v_{th,s} = \sqrt{2T_s/m_s}$, T_s is temperature in units of energy, and v is the total magnitude of the velocity $|\vec{v}|$. Assuming a square well approximation for the magnetic field and considering that the maximum magnetic field occurs at the mirror throat, the LBO has the form (Lenard & Bernstein 1958)

$$\mathcal{L}(f_s) = \nu_{sLBO} \frac{\partial}{\partial \vec{v}} \cdot \left(\vec{v} f_s + \frac{v_{th,s}^2}{2} \frac{\partial f_s}{\partial \vec{v}} \right), \quad (2.5)$$

where ν_{sLBO} is the collision frequency used in the LBO, \vec{v} is a velocity vector, and $v_{th,s}$ is the thermal velocity. Generality is left in defining the collision frequency ν_{sLBO} because it may be chosen to match certain important physical quantities and rates in its specific implementation (Francisquez *et al.* 2022). For instance, one may choose the collision frequency for the LBO to match thermal equilibration rates, Braginskii heat fluxes, or the Spitzer resistivity. Later in this work, we will investigate choosing the LBO's collision frequency to match ambipolar collisional losses from a magnetic mirror field. To simplify the analysis, we adopt the following normalizations and definitions:

$$\bar{v} = \frac{v}{v_{th,s}}; \quad F_s = \frac{v_{th,s}^3 f_s}{n_s}. \quad (2.6)$$

Our normalization \bar{v} is what Pastukhov (1974) and others refer to as x . We restate the LBO in normalized spherical coordinates to improve clarity,

$$\mathcal{L}(F_s) = \frac{1}{\bar{v}^2} \frac{\partial}{\partial \bar{v}} \bar{v}^3 \left(F_s + \frac{1}{2\bar{v}} \frac{\partial F_s}{\partial \bar{v}} \right) + \frac{Z_s}{2\bar{v}^2} \frac{\partial}{\partial \mu} (1 - \mu^2) \frac{\partial F_s}{\partial \mu}. \quad (2.7)$$

We introduce a factor Z_s into the diffusion term to correct for the LBO's approximation of treating the pitch-angle scattering and energy diffusion terms equally. Although for the LBO $Z_s = 1$, an opportunity is left for future work to correct this defect by modifying the coefficient Z_s . An essential distinction between equation (2.7) and the collision operators proposed by Pastukhov (1974) and Najmabadi *et al.* (1984) lies in the factors of \bar{v} . The collision operators in their work retain the velocity dependence within the Rosenbluth potentials. Below are the collision operators from Pastukhov (1974) and Najmabadi *et al.* (1984),

$$\mathcal{L}_{\text{Najmabadi}}(F_s) = \frac{1}{\bar{v}^2} \frac{\partial}{\partial \bar{v}} \left(F_s + \frac{1}{2\bar{v}} \frac{\partial F_s}{\partial \bar{v}} \right) + \frac{1}{\bar{v}^3} \left(Z_{s,N} - \frac{1}{4\bar{v}^2} \right) \frac{\partial}{\partial \mu} (1 - \mu^2) \frac{\partial F_s}{\partial \mu}, \quad (2.8)$$

$$\mathcal{L}_{\text{Pastukhov}}(F_s) = \frac{1}{\bar{v}^2} \frac{\partial}{\partial \bar{v}} \left(F_s + \frac{1}{2\bar{v}} \frac{\partial F_s}{\partial \bar{v}} \right) + \frac{1}{\bar{v}^3} \frac{\partial}{\partial \mu} (1 - \mu^2) \frac{\partial F_s}{\partial \mu}. \quad (2.9)$$

where $Z_{s,N}$ is the Z that is used in Najmabadi *et al.* (1984) and N stands for Najmabadi

et al. (1984), detailed in appendix B. To compare, the collision operator used in Pastukhov (1974) treats the factor in equation (2.8) ($Z_{s,N} - 1/(4\bar{v}^2)$) as one, although Cohen *et al.* (1986) addresses this limitation in treating the multi-species collisions. Comparing equation (2.8) and equation (2.7), we see that the drag and parallel diffusion are missing the $1/\bar{v}^3$ scaling of the more accurate collision operators. However, the pitch angle scattering term is not as bad, scaling like $1/\bar{v}^2$ for the LBO and like $1/\bar{v}^3$ for the more accurate operators.

To simplify the solution, we define a general form for the image problem. We impose that the image sinks start at velocity a , are placed solely outside the loss hyperboloid ($a > \bar{v}_0$ where $\bar{v}_0^2 = z_s e \phi / T_s$), and are isolated to lie along $\mu = \pm 1$ to preserve the symmetry of the problem. As described in figure 1,

$$Q(\bar{v}, \mu) = -\frac{\delta(1 - \mu^2)}{4\pi} H(\bar{v} - a) q(\bar{v}), \quad (2.10)$$

where $H()$ is the Heaviside step function and $\delta()$ is the Dirac delta function.

In Pastukhov (1974), they assume a form for the sinks $q(\bar{v}) = q_0 \exp(-\bar{v}^2)$, but the later work by Najmabadi *et al.* (1984) shows that defining $q(\bar{v}) = q_0 \exp(-\bar{v}^2)(Z_a - 1/4\bar{v}^2)/\bar{v}^3$ makes the resultant equations simpler to solve with fewer approximations. Najmabadi *et al.* (1984) finds the form of $q(\bar{v})$ by leaving its functional form free during the problem setup, then choosing a specific form at a later stage to facilitate a solution. Thus, we choose to leave the form of $q(\bar{v})$ arbitrary in equation (2.10) and will define its form at a later stage.

Without approximation, we can use equation (2.7) to rewrite equation (2.2) in the following way.

$$\frac{2e^{\bar{v}^2}}{\bar{v}} \frac{\partial}{\partial e^{\bar{v}^2}} \bar{v}^3 \frac{\partial}{\partial e^{\bar{v}^2}} \left(e^{\bar{v}^2} F_s \right) + \frac{Z_s}{2\bar{v}^2} \frac{\partial}{\partial \mu} (1 - \mu^2) \frac{\partial F_s}{\partial \mu} + Q(\bar{v}, \mu) = 0. \quad (2.11)$$

The inverse chain rule is used to absorb factors of \bar{v} into the derivatives, and we also employ the identity $F_s + (1/2\bar{v})\partial_{\bar{v}} F_s = (1/2\bar{v}) \exp(-\bar{v}^2) \partial_{\bar{v}} (\exp(\bar{v}^2) F_s)$. Let us define here the variable transformation $z(\bar{v}) = \exp(\bar{v}^2)$. We now make a critical approximation: large changes in z cause only small changes in $\bar{v}^2 = \ln(z)$, making the derivatives of powers of \bar{v} small. This justifies moving the \bar{v}^3 outside the derivative. In more detail, the approximation we make says

$$3\bar{v}^2 F_s, \bar{v} \frac{\partial F_s}{\partial \bar{v}} \ll \bar{v}^3 \frac{\partial F_s}{\partial \bar{v}}, \bar{v}^3 \frac{\partial}{\partial \bar{v}} \left(\frac{1}{2\bar{v}} \frac{\partial F_s}{\partial \bar{v}} \right). \quad (2.12)$$

This is valid since we are only interested in F_s near the loss cone at large velocities, where $\partial F_s / \partial \bar{v}$ is large and $\bar{v} \ll \bar{v}^3$. To simplify further, we define $g(\bar{v}, \mu) = \pi^{3/2} \exp(\bar{v}^2) F_s(\bar{v}, \mu)$ to factor out the Maxwellian component of the solution. This leads to the new form

$$\left(\frac{\partial^2}{\partial z^2} + \frac{Z_s}{4z^2 \ln(z)^2} \frac{\partial}{\partial \mu} (1 - \mu^2) \frac{\partial}{\partial \mu} \right) g_s(\bar{v}, \mu) + \frac{\pi^{3/2}}{2z \ln(z)} Q(\bar{v}, \mu) = 0. \quad (2.13)$$

We aim to make the operator on $g(\bar{v}, \mu)$ resemble a cylindrical Laplacian to map this problem to a Poisson problem. For this reason, we must also perform a transformation on the pitch angle scattering component. Consider a general variable transform of the form $\rho(\bar{v}, \mu) = h(\bar{v}, \mu) \sqrt{1 - \mu^2}$. Assuming a large mirror ratio $R \gg 1$, we may approximate that near the loss cone $\mu \approx \pm 1$. Thus, computing $\partial \rho / \partial \mu$, we neglect $\partial h / \partial \mu$. From this, we find $\partial_\mu \approx -(\mu h^2 / \rho) \partial_\rho$ and $(1 - \mu^2) = \rho^2 / h^2$. Under this transformation $(1 - \mu^2) \partial_\mu$ becomes $-\mu \rho \partial_\rho$ without any factors of $h(\bar{v}, \mu)$.

Part of the elegance of this method is that we are not limited by the form of $h(\bar{v}, \mu)$,

as long as z is only a function of \bar{v} . If $\partial_\mu z$ were non-zero, we would have to use the chain rule and compute $\partial_\mu \rho(z, \mu) = \partial_z \rho \partial_\mu z + \partial_\mu \rho$, thus complicating the procedure. This insight is perhaps the most pivotal innovation in Najmabadi *et al.* (1984) compared to the variable transformations presented in Pastukhov (1974). Pastukhov (1974) uses a variable transformation $z = \exp(\bar{v}^2)\mu/\sqrt{2\bar{v}^2}$ and $\rho = \exp(\bar{v}^2)\sqrt{1-\mu^2}$ where both variable transformations are functions of \bar{v} and μ . When ultimately satisfying boundary conditions, this leads Pastukhov (1974) to do “a number of straightforward but rather cumbersome algebraic transformations.” The complications arise due to the prefactors in front of the logarithm in their equation (17) having a factor of \bar{v}/μ , which comes from the μ/\bar{v} in their variable transformation for z . In contrast, Najmabadi *et al.* (1984) uses the variable transformations $z = \exp(\bar{v}^2)$ and $\rho = \sqrt{2\bar{v}^2/(Z_a - 1/4\bar{v}^2)} \exp(\bar{v}^2) \tan \theta$. Notice that, as we have pointed out above, the variable transformation in z does not depend on μ . The equivalent solution is Najmabadi *et al.* (1984) equation (23), which is divided by a Maxwellian compared to Pastukhov (1974) equation (17). Najmabadi *et al.* (1984) equation (23) has a mere constant before the logarithm, making satisfying boundary conditions much simpler.

By setting $h(\bar{v}, \mu)$ to cancel any factor in front of the pitch-angle scattering derivatives, it can be shown that the appropriate variable transformation is

$$\rho(\bar{v}, \mu) = \frac{2z \ln(z)}{\sqrt{Z_s}} \frac{\sqrt{1-\mu^2}}{\mu} = \frac{2z \ln(z)}{\sqrt{Z_s}} \tan \theta. \quad (2.14)$$

As a result, the problem is in the form of a cylindrical Poisson equation,

$$\frac{1}{\rho} \frac{\partial}{\partial \rho} \left(\rho \frac{\partial}{\partial \rho} g_s \right) + \frac{\partial^2 g_s}{\partial z^2} = \frac{\pi^{3/2}}{2z \ln(z)} \frac{\delta(1-\mu^2)}{4\pi} q(\bar{v}) H(\bar{v} - a). \quad (2.15)$$

We can now set the free function $q(\bar{v})$ such that the equation takes an ad-hoc, easy-to-solve form,

$$\frac{1}{\rho} \frac{\partial}{\partial \rho} \left(\rho \frac{\partial}{\partial \rho} g_s \right) + \frac{\partial^2 g_s}{\partial z^2} = \frac{\delta(\rho)}{2\pi\rho} 4\pi q_0 H(z - z_a). \quad (2.16)$$

On the right-hand side of equation (2.16), q_0 is equivalent to a constant linear charge density and $z_a = \exp(a^2)$. Although we choose q_0 to be a constant for the sake of having an easy-to-solve problem, it does mean we are sacrificing some detail in the ability to match equation (2.1) perfectly; however, exact matching is not necessary because the distribution function, as well as losses, decay at higher energies and the majority of particles are lost near the tip of the loss hyperboloid so that is the region we are most interested in matching. By matching equations (2.15) and (2.16), we show in Appendix A that the appropriate connection between $q(\bar{v})$ and q_0 is

$$q(\bar{v}) = q_0 \cdot \frac{8}{\sqrt{\pi}} \frac{\mu^2 Z_s}{z \ln(z)}. \quad (2.17)$$

With the new coordinates ρ and z , we transform boundary condition (2.4). In addition, the lower limit of $z = 1$ for $\bar{v} = 0$ is extended to $z = 0$ since $z \equiv \exp(\bar{v}^2) \gg 1$ or set $z' = \exp(\bar{v}^2) - 1 = z(1 + O(\exp(-\bar{v}^2)))$.

$$g_s(\rho, z)|_{z=0} = 1 \quad (2.18)$$

Equation (2.16) with boundary condition (2.18) is solved in Jackson (1999). The equivalent problem in electricity and magnetism terms is having a conducting boundary condition on the $z = 0$ plane held at potential $g_s = 1$ and placing a wire of constant

linear charge density q_0 on the z -axis, suspended above the $z = 0$ plane by height $z = z_a$. The standard method of solving this problem is to use the method of images to match the conducting boundary condition. This use of the method of images for the equivalent Poisson problem after previously using the method of image approach to place image sources and sinks in figure 1 is why this approach is referred to as the method of images solution for determining loss rates from a magnetic mirror. Only requiring unmapping the equation through stated variable transformations, we find the appropriate distribution function for a magnetic mirror as

$$g_s(\rho, z) = 1 - q_0 \ln \left(\frac{z_a + z + \sqrt{\rho^2 + (z_a + z)^2}}{z_a - z + \sqrt{\rho^2 + (z_a - z)^2}} \right). \quad (2.19)$$

Mapping this problem back to the magnetic mirror and using that $z \gg 1$ near the loss hyperboloid, we can apply the boundary conditions assigned to this problem in equation (2.3). Interestingly, this is the only part of the calculation in which information about the magnetic field is used in the solution. We show in Appendix C that for a general variable transformation $z = \exp(\bar{v}^2)$, $\rho = \bar{\rho}(\bar{v})z \tan \theta$, we get

$$q_0 = \left(\ln \left(\frac{w+1}{w-1} \right) \right)^{-1} \quad (2.20)$$

$$w^2 = 1 + \frac{\bar{\rho}(\bar{v}_0)^2}{2R\bar{v}_0^2} = 1 + \frac{2\bar{v}_0^2}{Z_s R} \quad (2.21)$$

where $w = \exp(a^2 - \bar{v}_0^2)$. This can be inverted to give $a^2 = \bar{v}_0^2 + \ln(w)$, which determines the edge of the sink region, a , in terms of the tip of the loss region v_0 . Note that $\bar{\rho}$ is different than the factor of h mentioned earlier. To calculate this system's confinement time and energy loss rate, we integrate the image sinks over all velocity space, considering the symmetry in gyro- and pitch-angle.

$$\frac{1}{n_s \nu_{sLBO}} \frac{dn_s}{dt} = 2\pi \int_0^\infty \bar{v}^2 d\bar{v} \int_{-1}^1 d\mu Q(\bar{v}, \mu) \quad (2.22)$$

$$\frac{3}{2} \frac{1}{\nu_{sLBO}} \frac{1}{n_s T_s} \frac{dn_s T_s}{dt} = 2\pi \int_0^\infty \bar{v}^4 d\bar{v} \int_{-1}^1 d\mu Q(\bar{v}, \mu) \quad (2.23)$$

Although this appears to be a straightforward integral, there is a subtlety to handling it worth mentioning. Equation (2.22) appears as if it is integrating over half of each delta function on both sides, but it is, in fact, integrating two whole peaks of the delta function across all of velocity space, so $\int_{-1}^1 \delta(1 - \mu^2) d\mu = 1$. Once accounting for this intricacy, we arrive at the following forms for confinement time and energy loss rate.

$$\frac{1}{\tau_c} = \frac{1}{n_s} \frac{dn_s}{dt} = -\nu_{sLBO} 2Z_s \frac{\text{Erfc}(a)}{\ln \left(\frac{w+1}{w-1} \right)}, \quad (2.24)$$

$$\frac{1}{E_s} \frac{dE_s}{dt} = \frac{1}{n_s T_s} \frac{d(n_s T_s)}{dt} = -\nu_{sLBO} \frac{4}{3\sqrt{\pi}} Z_s \frac{e^{-a^2} a + \frac{\sqrt{\pi}}{2} \text{Erfc}(a)}{\ln \left(\frac{w+1}{w-1} \right)}. \quad (2.25)$$

Here, τ_c is the confinement time, $E_s = 3/2 n_s T_s$ is total energy of the system, $\text{Erfc}()$ is the complementary error function, $w = \sqrt{1 + 2z_s e\phi / (T_s Z_s R)}$, and $a = \sqrt{z_s e\phi / T_s + \ln(w)}$.

We proceed to calculate the energy of the particle, but due to collisions, $z_s e\phi / T_s \sim (1/2) \ln(m_i/m_e) \gg 1$. Furthermore, for $R \gg z_s e\phi / T_s Z_s$, $\ln(w)$ is small, giving $a \simeq$

$\sqrt{z_s e \phi / T_s} \gg 1$. The asymptotic expansion for a large argument of the complementary error function is $\text{Erfc}(x) \approx \exp(-x^2) / (\sqrt{\pi} x) \times (1 - 1/2x^2 + 3/4x^4 + \mathcal{O}(1/x^6))$, so τ_c scales as $a \exp(a^2)$. The average energy of lost particles is found by evaluating $E_{s,\text{loss}} = (dE_s/dt)/(dn_s/dt)$.

$$\frac{E_{s,\text{loss}}}{T_s} = \frac{1}{2} \left(1 + \frac{2ae^{-a^2}}{\sqrt{\pi}\text{Erfc}(a)} \right) \quad (2.26)$$

$$\approx a^2 + 1 - \frac{1}{2a^2} + \mathcal{O}(1/a^4) \quad (2.27)$$

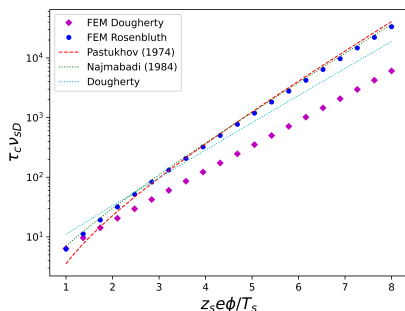
It is important to note that equation (2.24) and subsequent definitions are presented in their un-normalized form. During the un-normalization process, all quantities are stated in terms of the temperature T_s of the species. This avoids confusion when using a different normalization procedure for the thermal velocity.

3. Numerical simulations and corrections to equation (2.20)

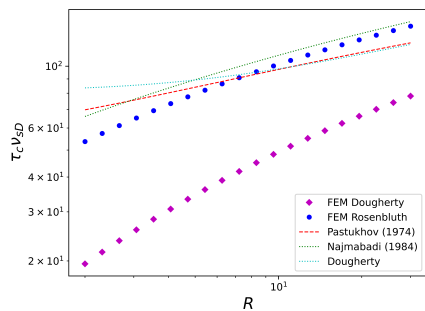
We compare our approximate expressions for the loss rates in magnetic mirrors to results obtained utilizing a code based on the work of Ochs *et al.* (2023). The code uses the FEniCS DolfinX Python package to employ the finite element method (FEM) with third-order continuous Galerkin discretization to solve a general Fokker-Planck model collision operator. The FEM model is meshed over the upper right quadrant of \bar{v}, θ space and has a low-energy source of the form $\bar{v}^2 \exp(-\bar{v}^2/\bar{v}_{s0}^2)\theta^2(\pi/2 - \theta)^{\dagger}$. Here, \bar{v} is normalized velocity, and θ is pitch angle. The normalized thermal velocity for the source is evaluated at $\bar{v}_{s0} = 0.2$ to concentrate it at low energy. This source form is chosen to go to zero on the boundaries smoothly (the precise form of the source term has little effect on the results in the asymptotic limit $z_s e \phi / T_e \gg 1$). Neumann boundary conditions ($f'_s = 0$) are used at $\theta = 0$, $\theta = \pi/2$, $v = 0$, and $v = v_{max}$, the maximal velocity extent in the problem. The boundary condition on the loss hyperboloid is Dirichlet ($f_s = 0$). The domain is extended $2z_s e \phi / T_s$ past the loss hyperboloid vertex and the simulation converges to a stable solution within 1% variation with a mesh size of $\Delta\bar{v} = \Delta\theta = 0.1$ with double resolution near the loss hyperboloid and source.

To compare our numerical results to prior computational work, we need to make a key distinction between the collision operator utilized by our code in reproducing the results from Najmabadi *et al.* (1984) and the operators used in previous work. The results labeled ‘‘FEM Rosenbluth’’ utilize a slightly modified version of the collision operator in equation (2.8), whereas the code utilized in Cohen *et al.* (1978) and later utilized in Najmabadi *et al.* (1984) and Fyfe *et al.* (1981) considers a multi-species Fokker-Planck equation derived from non-linear isotropic Rosenbluth potentials. Naive implementation of equation (2.8) would violate the assumption that $\bar{v} \gg 1$ because our domain also includes low velocities. To compensate, we approximate the parallel drag-diffusion frequency in equation (2.8) by utilizing a Pad e approximation of the form $1/v^3 \rightarrow 1/(1+v^3)$, which asymptotically matches the high- and low-velocity Rosenbluth limits. For the pitch angle scattering component, we have a full calculation of the pitch angle scattering rate while considering collisions on a Maxwellian background to keep the problem linear. We consider two cases: electron collisions with a hydrogen background and hydrogen collisions on an electron background. In both cases, the thermal velocity of electrons is much higher than the thermal velocity of the hydrogen. This results in the

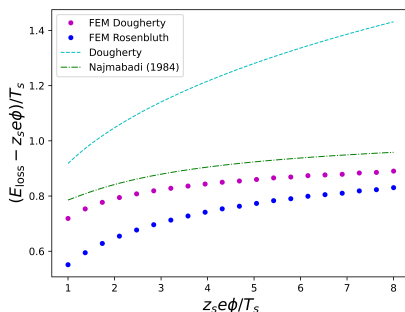
[†] There is a typo in Ochs (2023), where they miss a negative sign in the exponent.



(a) Confinement time variations with ambipolar potential for $R = 10$ for electrostatically confined electrons ($Z_{s,N} = 1$).



(b) Confinement time variations with mirror ratio for $z_s e \phi / T_s = 3$ for electrostatically confined electrons ($Z_{s,N} = 1$).



(c) Variation of average energy of lost electrons ($Z_{s,N} = 1$) with ambipolar potential for $R = 10$.

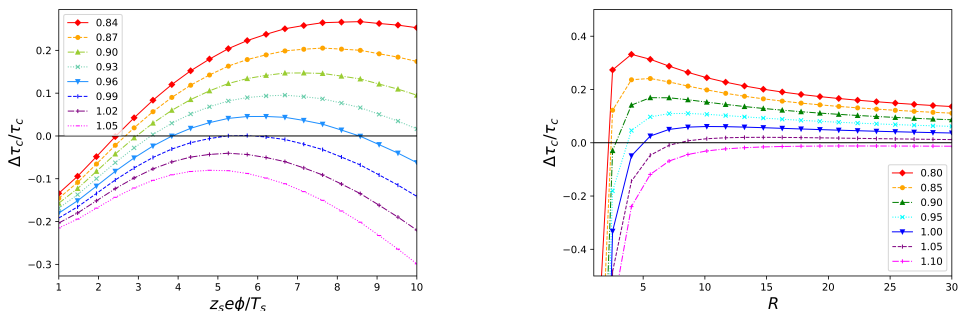
FIGURE 2. Normalized particle confinement time $\tau_c \nu_{sLBO}$ from equation (2.24) and its dependence on ambipolar potential and mirror ratio of the LBO versus [Pastukhov \(1974\)](#) and [Najmabadi *et al.* \(1984\)](#). The y-axis is confinement time, normalized to the collision frequency with $Z_s = 1$ for electrostatically confined electrons.

following collision operator.

$$\mathcal{L}_{\text{Code}}(F_s) = \frac{1}{\bar{v}^2} \frac{\partial}{\partial \bar{v}} \frac{\bar{v}^2}{1 + \bar{v}^3} \left(\bar{v} F_s + \frac{1}{2} \frac{\partial F_s}{\partial \bar{v}} \right) + \frac{1}{\bar{v}^3} P(v) \frac{\partial}{\partial \mu} (1 - \mu^2) \frac{\partial F_s}{\partial \mu}. \quad (3.1)$$

where $P(v) = (1 + \mathcal{R}(v))/2$ for electron collisions with a hydrogen background ($Z_{s,n} = 1$) and $P(v) = \mathcal{R}(v)/2$ for hydrogen collisions with an electron background ($Z_{s,n} = 1/2$) and $\mathcal{R}(v) = 1/(\sqrt{\pi}v) \exp(-v^2) + (1 - 1/2v^2) \text{Erf}(v)$ and Erf is the error function. In contrast, the LBO model is implemented in the code without approximations as equation (2.7).

In figure 2, the numerical model is validated by comparing the analytic results presented in [Pastukhov \(1974\)](#), [Najmabadi *et al.* \(1984\)](#), equation (2.24), and equation (2.26), which in turn were validated using other numerical methods. Results in figure 2 agree well with those in many prior works ([Najmabadi *et al.* 1984](#); [Cohen *et al.* 1978](#); [Fyfe *et al.* 1981](#)). The confinement time τ_c is normalized to collision frequency for generality. The diamonds are the finite element method numerical results, and the dashed lines are the analytic approximations. Although figure 2 shows great agreement with prior work, it has a poor agreement with equation (2.24). [Najmabadi *et al.* \(1984\)](#) overcome



(a) Confinement time errors with ambipolar potential for $R = 10$.

(b) Confinement time errors with mirror ratio for $z_s e\phi/T_s = 3$.

FIGURE 3. Fractional error in the confinement estimates between the numeric model and analytic approximation for electrostatically confined electrons. The legend goes from the top curve to the bottom curve in even steps in the value of c_0

this limitation by finding a correction coefficient in their equation (41b) based on the difference in flux from the approximate loss cone from the solution $g(\bar{v}, \mu)$ versus the real loss cone. We have not replicated the calculation used to determine their equation (41b), so instead, we opt to calculate this correction numerically. We look for a correction that adds a coefficient to equation (2.20) in the same place that Najmabadi *et al.* (1984) finds. We call this correction coefficient c_0 and it is chosen to minimize error with the finite element model. Equations (2.20), (2.24), and (2.25) are modified to be the following.

$$\frac{1}{\tau_c} = \frac{1}{n_s} \frac{dn_s}{dt} = -\nu_{sLBO} 2Z_s \frac{\text{Erfc}(a)}{\ln\left(\frac{w+1}{w-1}\right) - c_0}, \quad (3.2)$$

$$\frac{1}{E_s} \frac{dE_s}{dt} = \frac{1}{n_s T_s} \frac{d(n_s T_s)}{dt} = -\nu_{sLBO} \frac{4}{3\sqrt{\pi}} Z_s \frac{e^{-a^2} a + \frac{\sqrt{\pi}}{2} \text{Erfc}(a)}{\ln\left(\frac{w+1}{w-1}\right) - c_0}. \quad (3.3)$$

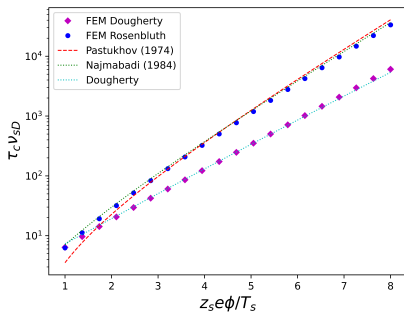
In figure 3, we show various curves that describe the error between equation (3.2) and the finite element model for various values of c_0 . This figure shows us that the value of c_0 that minimizes error with the finite element model depends on the ambipolar potential and mirror ratio under investigation, although it seems to asymptote to a single value for a sufficiently large mirror ratio and ambipolar potential. In table 1, we list the appropriate correction factor to use for various values of ambipolar potential and mirror ratio that minimize error with the loss rate from the finite element model.

Figure 2 is reconstructed in figure 4 using the correction coefficient c_0 in equations (3.2) and (3.3). In figure 4(c), a choice to not plot the results from Pastukhov (1974) is made due to their close agreements with the results from Najmabadi *et al.* (1984).

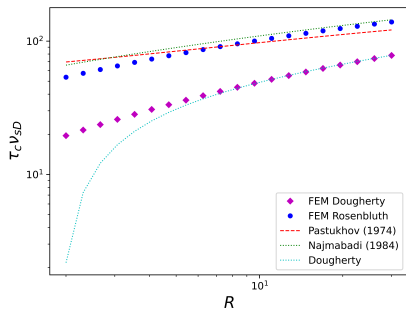
In comparing the dependence of the loss rate with ambipolar potential, figure 4(a) shows a key difference between the Fokker-Planck form Coulomb operator and the LBO. Using a constant mirror ratio of $R = 10$, the LBO alters the confinement time compared to the Fokker-Planck collision operator utilized in other studies (Khudik 1997; Najmabadi *et al.* 1984; Pastukhov 1974; Catto & Bernstein 1981; Catto & Li 1985). Particularly, the confinement time of Najmabadi *et al.* (1984) scales as $a^2 e^{a^2}$, but equation (3.2) scales

$z_s e\phi/T_s$	R									
	5	10	15	20	25	30	35	40	45	50
1	1.305	1.310	1.302	1.295	1.288	1.283	1.278	1.274	1.271	1.268
2	1.066	1.094	1.093	1.087	1.080	1.075	1.069	1.065	1.060	1.057
3	1.004	1.066	1.078	1.080	1.077	1.074	1.070	1.066	1.062	1.059
4	0.967	1.057	1.084	1.093	1.095	1.095	1.093	1.091	1.088	1.085
5	0.933	1.044	1.083	1.099	1.107	1.109	1.110	1.109	1.108	1.106
6	0.900	1.027	1.077	1.100	1.112	1.118	1.121	1.122	1.121	1.120
7	0.869	1.007	1.065	1.093	1.109	1.117	1.122	1.125	1.126	1.126
8	0.840	0.987	1.052	1.085	1.104	1.115	1.122	1.126	1.128	1.129
9	0.813	0.968	1.038	1.077	1.099	1.113	1.122	1.128	1.132	1.134
10	0.963	0.948	1.023	1.065	1.090	1.106	1.117	1.124	1.129	1.132

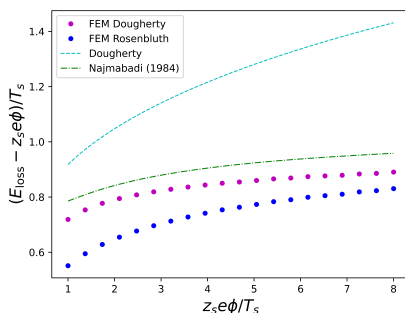
TABLE 1. A table of optimal correction factors c_0 for various values of $z_s e\phi/T_s$ and R to minimize error with the finite element model for $Z_s = 1$.



(a) Confinement time variations with ambipolar potential for $R = 10$, $c_0 = 1.04$, $Z_{s,N} = 1$.



(b) Confinement time variations with mirror ratio for $z_s e\phi/T_s = 3$ and $c_0 = 1.07$, $Z_{s,N} = 1$.



(c) Variation of average energy of lost particles with ambipolar potential for $R = 10$, $c_0 = 1.04$, $Z_{s,N} = 1$.

FIGURE 4. Comparison particle confinement time and average loss energy, and its dependence on ambipolar potential and mirror ratio of the LBO versus [Pastukhov \(1974\)](#) and [Najmabadi et al. \(1984\)](#). The y-axis is confinement time or average loss energy subtracted by $z_s e\phi/T_s$, normalized to the collision frequency with $Z_s = 1$ for electrostatically confined electrons.

as ae^{α^2} . This scaling difference makes sense because the LBO overestimates the collision frequency and ignores the collisionality drop-off with velocity.

Figure 4(a) and 4(b) compare the variation with potential and mirror ratio of the loss ratios calculated using different collision operators. We see that the LBO model underestimates the confinement time at all potentials and mirror ratios. Even so, the percentage variation of loss rate upon modification of the mirror ratio has similar trends in the finite element model when comparing the LBO model to equation (3.1). Furthermore, each numerical line matches their respective analytic curves well, validating the models. Figure 4(b) leads us to conclude that there is no significant difference in the dependence of loss rate on mirror ratio when considering LBO collisions.

Figure 4(c) shows that our equation (2.26) and the numerical approach exhibit similar trends, but are very different in magnitude. It is important to note that figure 4(c) subtracts the linear component $z_s e\phi/T_s$ to highlight the differences between the different results. Comparing results to prior work, our numerical method produces roughly a 20% difference with respect to the analytic results from Najmabadi *et al.* (1984). Although errors of 20% are large, Najmabadi *et al.* (1984) noticed similar errors, so these results are comparable to prior work. Interestingly, while the analytic results of Najmabadi *et al.* (1984) seem to have a constant 20% error, the discrepancy between (2.26) and the numerical results grows with $z_s e\phi/T_s$. Similar errors of 20% are observed at low values of $z_s e\phi/T_s$; at large values, the error grows to nearly 100% at $z_s e\phi/T_s = 8$. The LBO model has an overall higher average loss energy than the model used by Najmabadi *et al.* (1984). This means the losses from LBO collisions are more spread around the loss hyperboloid. In contrast, a more accurate collision operator would have losses more concentrated around the tip of the loss hyperboloid. It is worth noting that the correction factor c_0 does not modify equation (2.26).

4. Discussion

We suggest that codes using an LBO/Dougherty collision operator improve their results by scaling the collision frequency used to obtain the correct mirror confinement time and ambipolar potential. First, one must obtain an accurate estimate of the ambipolar potential of the system. The ambipolar potential may be determined using the analytic results presented in Najmabadi *et al.* (1984) or in a code such as our finite element solver or the one presented in Egedal *et al.* (2022). Using this accurate estimate of ambipolar potential, one can calculate the estimated confinement time using the results from Najmabadi *et al.* (1984), presented in appendix B. Call this confinement time τ_N . Now that we have calculated the ambipolar potential and confinement time, we may invert equation (3.2) to determine $\nu_{sLBO}Z_s$, with the appropriate correction coefficient using table 1,

$$\frac{1}{\nu_{sLBO}Z_s} = 2\tau_{c,N} \left(\ln \left(\frac{w+1}{w-1} \right) - c_0 \right)^{-1} \text{Erfc}(a), \quad (4.1)$$

Here, recall that $w = \sqrt{1 + 2z_s e\phi / (T_s Z_s R)}$, and $a = \sqrt{z_s e\phi / T_s + \ln(w)}$. The simplest approach to achieving the correct results is to scale the collision frequency, setting $Z_s = 1$, which will also have undesirable effects such as modifying multi-species thermal equilibration times (Francisquez *et al.* 2022). Let us define a collision frequency gain constant $\gamma = \nu_{sLBO}/\nu_N$ where ν_N is the collision frequency used in the results of Najmabadi *et al.* (1984). One must scale the collision frequency ν_N by a factor of γ for the loss rate of the system using the LBO to be equal to the system using the operator from Najmabadi *et al.* (1984). Alternatively, one could implement an LBO with

a modified diffusion coefficient, including Z_s . Then, one may scale Z_s by a factor of γ instead of collision frequency, which may be preferable depending on the situation. $Z_s \neq 1$ corresponds to an anisotropic collision operator, which can be more accurate but, in some cases, can be numerically more challenging (Sharma & Hammett 2011).

Putting this into practice, we make suggestions of the appropriate scaling factor γ for WHAM and WHAM++. Egedal *et al.* (2022) predicts an ambipolar potential of $z_s e\phi/T_e \simeq 5$ for WHAM and WHAM++. For WHAM, $R = 13.3$ and $\gamma = 0.1788$, and for WHAM++, $R = 10$ and $\gamma = 0.1622$ with $c_0 = 1.05$ for both machines. It makes sense that the LBO would need a diminished frequency to match Najmabadi's loss rate and the $1/v^3$ drop-off in collisionality at large velocity.

The scrape-off layer of toroidal confinement devices, like tokamaks and stellarators, can exhibit a Pastukhov potential due to the difference in magnetic field strength between the inboard and outboard sides (Majeski *et al.* 2017). The magnetic field magnitude ($|B|$) varies inversely with the distance (R) from the central axis, determining the mirror ratio ($R_{\text{out}}/R_{\text{in}}$) of these devices, typically around 2. Additionally, observed potentials are approximately $z_s e\phi/T \sim 2$. This implies these devices have low mirror ratios and a limited potential. In this scenario, figure 4(a) aligns reasonably with previous findings by Najmabadi *et al.* (1984). However, Pastukhov (1974) and Najmabadi *et al.* (1984) consider a high mirror ratio and potential limit, making their results inaccurate for toroidal confinement devices. Caution is necessary when applying these equations in regimes approaching the bounds of these limits. The variational method for studying collisional losses not considered here offers an approach suitable for arbitrary mirror ratios and ambipolar potential, making results from Catto & Li (1985) and Khudik (1997) more appropriate. In this limit, there is no significant difference between the collisional losses due to a Dougherty / LBO operator and those produced using a more accurate one.

We note a subtlety in the problem setup here. It is usually stated that there is a source of particles and energy at low energy to balance the sink at high energy. Standard electron-electron collision operators are energy conserving, and the electron-ion collision operator has been approximated by pitch angle scattering, which also conserves energy, so one may wonder where the energy injection comes from. It should be noted that it is not sufficient to add a source to the kinetic equation of the form $S(v) = S_0 \delta(v - v_I)/(4\pi v^2)$ (where S_0 is the source rate in units of particles per second per unit volume), because no choice of the injection velocity v_I can provide enough power for steady state unless v_I is quite large, violating the assumption that the source is at low energy. This is because the source energy per injected particle, $(1/2)mv_I^2$, must be the same in steady state as the average energy per particle lost, which from (2.27) is $E_{\text{loss}} \sim z_s e\phi \gg T_e$.

The resolution to this issue is as follows: in a real mirror machine, the heating of electrons comes from collisions with beam and bulk ions (typically much hotter than the electrons) or RF heating. Collisions and quasilinear RF heating can be roughly modeled here by slightly increasing the velocity diffusion coefficient in the collision operator, i.e. slightly increasing the factor of $v_{\text{th},s}^2$ that appears in the Dougherty-Lenard-Bernstein collision operator ((2.5)) above the actual thermal velocity squared $\langle v^2 \rangle/3$ one would find from distribution function. Because the mirror confinement time τ_c is much longer than the collision time in the asymptotic regime we are studying, roughly by a factor of $\sim \exp(a^2) \sim \exp(z_s e\phi/T_e) \gg 1$ (neglecting factors of a or a^2 depending on the choice of collision operator), the velocity diffusion coefficient only needs to be increased slightly (the relative change scales as $\exp(-z_s e\phi/T_e) \ll 1$). In numerical codes, this is sometimes implemented via a hidden assumption by not literally using an energy-conserving electron-electron collision operator and instead fixing the value of $v_{\text{th},s}^2$ in the

diffusion coefficient as an input parameter. One would find that the actual $\langle v^2 \rangle / 3$ from the distribution function is slightly less than the input parameter. Some calculations do the same thing by normalizing the velocity variable to a fixed parameter, which will turn out to be slightly higher than the actual thermal velocity. Nevertheless again, this is a tiny correction in the asymptotic limit.

5. Conclusion

In summary, this study delves into the critical role that collisions play in governing particle and energy transport within magnetic mirror confinement systems. We use an LBO model to proceed through the method of images calculation to investigate particle and energy confinement. Notably, we address the challenges posed when using a different collision operator compared to prior work.

A pivotal observation emerges when examining the dependence of confinement time on the ambipolar potential, as depicted in figure 4(a). The LBO alters the particle confinement time compared to more accurate collision operators utilized in earlier research (Khudik 1997; Najmabadi *et al.* 1984; Pastukhov 1974; Catto & Bernstein 1981; Catto & Li 1985). Notably, our findings demonstrate that the particle confinement time scales like $a \exp(a^2)$ using the LBO, whereas a more accurate collision operator would yield $a^2 \exp(a^2)$, where a^2 is approximately the normalized ambipolar potential, $z_s e \phi / T_e$ (see the inline equations after equation (2.25)). This scaling discrepancy is attributed to the LBO's disregard for the drop-off in collisionality with velocity. Figure 4(b) highlights that despite significantly different loss rates at the same potential, the scaling behavior with the mirror ratio remains comparable with prior models. Finally, figure 4(c) showcases that equation (3.3) reproduces comparable errors compared to prior work.

To address these findings, we propose a practical modification for codes utilizing an LBO or Dougherty operator to achieve the correct ambipolar potential. This involves estimating the particle loss rate, then calculating the ambipolar potential from a code or predictions from Najmabadi *et al.* (1984). Equation (3.2) can then be employed to determine the appropriate scaling factor for the collision frequency or pitch angle scattering enhancement, ensuring congruence with the electron confinement time. This scaling factor, denoted as γ , depends on various parameters, including the correction factor c_0 , which can be interpolated from table 1.

Numerous avenues for extending this research exist. Firstly, the incorporation of anisotropic diffusion coefficients has the potential to alleviate the approximations inherent in the LBO operator. This is facilitated by the presence of Z_s in equations (3.2) and (3.3). Additionally, we have expanded the method of images approach to accommodate alternative forms of the Fokker-Planck coefficients used in the collision operator. Future investigations could explore alternative approximate collision operators using this generalized approach or even take the approximations from Najmabadi *et al.* (1984) to higher order. In addition, the code could be improved by including an improved approximation to the energy diffusion term in equation (3.1) using the Rosenbluth potentials. Furthermore, future research endeavors might delve into variational techniques, as demonstrated by Catto & Bernstein (1981), Catto & Li (1985), and Khudik (1997), to relax the constraints imposed by large mirror ratios within the method of images. On the computational side, it would be interesting to see how much the results of Francisquez *et al.* (2023) change with rescaling the collision frequency suggested here. Extending the lessons learned here beyond magnetic mirrors, it is worth considering tokamak and stellarator confinement systems. As discussed, toroidal confinement systems exist in the space of low mirror ratios and low potentials, which we studied to be a regime where the loss rate due to LBO

collisions has a reasonable agreement with more comprehensive collision operators, and little modification needs to be made. However, this analysis assumed large mirror ratios and large potentials, so more careful analysis must be done using variational techniques for a complete answer.

6. Acknowledgements

The authors thank Ammar Hakim, Manaure Francisquez, and Igor Kaganovich for their helpful discussions culminating in the ideas presented here. This work was supported by Princeton University and the U.S. Department of Energy under contract number DE-AC02-09CH11466. The United States Government retains a non-exclusive, paid-up, irrevocable, world-wide license to publish or reproduce the published form of this manuscript, or allow others to do so, for United States Government purposes. W.S. was supported by a grant from the Simons Foundation/SFARI (560651, AB) and DoE Grant No. DE-AC02-09CH11466.

REFERENCES

- BAGRYANSKY, P.A., ANIKEEV, A.V., BEKLEMISHEV, A.D., DONIN, A.S., IVANOV, A.A., KORZHAVINA, M.S., KOVALENKO, YU V., KRUGLYAKOV, E.P., LIZUNOV, A.A., MAXIMOV, V.V. & OTHERS 2011 Confinement of hot ion plasma with $\beta = 0.6$ in the gas dynamic trap. *Fusion Science and Technology* **59** (1T), 31–35.
- BAGRYANSKY, P. A., SHALASHOV, A. G., GOSPODCHIKOV, E. D., LIZUNOV, A. A., MAXIMOV, V. V., PRIKHODKO, V. V., SOLDATKINA, E. I., SOLOMAKHIN, A. L. & YAKOVLEV, D. V. 2015 Threefold increase of the bulk electron temperature of plasma discharges in a magnetic mirror device. *Phys. Rev. Lett.* **114**, 205001.
- BEKLEMISHEV, A. D. 2017 Tail-Waving System for Active Feedback Stabilization of Flute Modes in Open Traps. *Fusion Science and Technology* **59** (1T), 90–93.
- BEKLEMISHEV, ALEXEI D., BAGRYANSKY, PETER A., CHASCHIN, MAXIM S. & SOLDATKINA, ELENA I. 2010 Vortex confinement of plasmas in symmetric mirror traps. *Fusion Science and Technology* **57** (4), 351–360.
- BERK, H.L. & CHEN, C.Y. 1988 Dissipative trapped particle modes in tandem mirrors. *The Physics of Fluids* **31** (1), 137–148.
- CATTO, PETER J. & BERNSTEIN, IRA B. 1981 Collisional end losses from conventional and tandem mirrors. *The Physics of Fluids* **24** (10), 1900–1905.
- CATTO, PETER J. & LI, XING ZHONG 1985 Particle loss rates from electrostatic wells of arbitrary mirror ratios. *The Physics of Fluids* **28** (1), 352–357.
- CELEBRE, G., SERVIDIO, S. & VALENTINI, F. 2023 Phase space dynamics of unmagnetized plasmas: Collisionless and collisional regimes. *Physics of Plasmas* **30** (9), 092304, arXiv: https://pubs.aip.org/aip/pop/article-pdf/doi/10.1063/5.0160549/18121857/092304_1_5.0160549.pdf.
- CHERNIN, D.P. & ROSENBLUTH, M.N. 1978 Ion losses from end-stoppered mirror trap. *Nuclear Fusion* **18** (1), 47.
- COHEN, BRUCE I., FREIS, ROBERT P. & NEWCOMB, WILLIAM A. 1986 Interchange, rotational, and ballooning stability of long-thin axisymmetric systems with finite-orbit effects. *The Physics of Fluids* **29** (5), 1558–1577.
- COHEN, R.H., RENSINK, M.E., CUTLER, T.A. & MIRIN, A.A. 1978 Collisional loss of electrostatically confined species in a magnetic mirror. *Nuclear Fusion* **18** (9), 1229.
- DOUGHERTY, J.P. 1964 Model Fokker-Planck equation for a plasma and its solution. *The Physics of Fluids* **7** (11), 1788–1799.
- EGEDAL, J., ENDRIZZI, D., FOREST, C.B. & FOWLER, T.K. 2022 Fusion by beam ions in a low collisionality, high mirror ratio magnetic mirror. *Nuclear Fusion* **62** (12), 126053.
- ENDRIZZI, D., ANDERSON, J.K., BROWN, M., EGEDAL, J., GEIGER, B., HARVEY, R.W., IALOVEGA, M., KIRCH, J., PETERSON, E., PETROV, YU V. & OTHERS 2023 Physics

- basis for the Wisconsin HTS Axisymmetric Mirror (WHAM). *Journal of Plasma Physics* **89** (5), 975890501.
- FOWLER, T.K., MOIR, R.W. & SIMONEN, T.C. 2017 A new simpler way to obtain high fusion power gain in tandem mirrors. *Nuclear Fusion* **57** (5), 056014.
- FRANCISQUEZ, MANAURE, BERNARD, TESS N., MANDELL, NOAH R., HAMMETT, GREGORY W. & HAKIM, AMMAR 2020 Conservative discontinuous Galerkin scheme of a gyro-averaged Dougherty collision operator. *Nuclear Fusion* **60** (9), 096021.
- FRANCISQUEZ, MANAURE, JUNO, JAMES, HAKIM, AMMAR, HAMMETT, GREGORY W & ERNST, DARIN R 2022 Improved multispecies Dougherty collisions. *Journal of Plasma Physics* **88** (3), 905880303.
- FRANCISQUEZ, MANAURE, ROSEN, MAXWELL H., MANDELL, NOAH R., HAKIM, AMMAR, FOREST, CARY B. & HAMMETT, GREGORY W. 2023 Toward continuum gyrokinetic study of high-field mirrors. *Physics of Plasmas* **30** (10).
- FREI, B.J., HOFFMANN, A.C.D. & RICCI, P. 2022 Local gyrokinetic collisional theory of the ion-temperature gradient mode. *Journal of Plasma Physics* **88** (3), 905880304.
- FYFE, D., WEISER, A., BERNSTEIN, I., EISENSTAT, S. & SCHULTZ, M. 1981 A finite element solution of a reduced Fokker-Planck equation. *Journal of Computational Physics* **42** (2), 327–336.
- GRANDGIRARD, V., ABITEBOUL, J., BIGOT, J., CARTIER-MICHAUD, T., CROUSEILLES, N., DIF-PRADALIER, G., EHRLACHER, CH., ESTEVE, D., GARBET, X., GHENDRIH, PH., LATU, G., MEHRENBARGER, M., NORSCINI, C., PASSERON, CH., ROZAR, F., SARAZIN, Y., SONNENDRÜCKER, E., STRUGAREK, A. & ZARZOSO, D. 2016 A 5d gyrokinetic full-f global semi-lagrangian code for flux-driven ion turbulence simulations. *Computer Physics Communications* **207**, 35–68.
- HAKIM, AMMAR, FRANCISQUEZ, MANAURE, JUNO, JAMES & HAMMETT, GREGORY W. 2020 Conservative discontinuous Galerkin schemes for nonlinear Dougherty–Fokker–Planck collision operators. *Journal of Plasma Physics* **86** (4), 905860403.
- HATCH, D. R., JENKO, F., BAÑÓN NAVARRO, A. & BRATANOV, V. 2013 Transition between saturation regimes of gyrokinetic turbulence. *Phys. Rev. Lett.* **111**, 175001.
- HIRSHMAN, S.P. & SIGMAR, D.J. 1976 Approximate Fokker–Planck collision operator for transport theory applications. *The Physics of Fluids* **19** (10), 1532–1540.
- HOFFMANN, A.C.D., FREI, B.J. & RICCI, P. 2023 Gyrokinetic simulations of plasma turbulence in a z-pinch using a moment-based approach and advanced collision operators. *Journal of Plasma Physics* **89** (2), 905890214.
- JACKSON, JOHN DAVID 1999 Classical electrodynamics.
- KHUDIK, V.N. 1997 Longitudinal losses of electrostatically confined particles from a mirror device with arbitrary mirror ratio. *Nuclear Fusion* **37**.
- KNYAZEV, A.R., DORF, M. & KRASHENINNIKOV, S.I. 2023 Implementation and verification of a model linearized multi-species collision operator in the cogent code. *Computer Physics Communications* **291**, 108829.
- LENARD, ANDREW & BERNSTEIN, IRA B. 1958 Plasma oscillations with diffusion in velocity space. *Physical Review* **112** (5), 1456.
- LOUREIRO, N.F., DORLAND, W., FAZENDEIRO, L., KANEKAR, A., MALLET, A., VILELAS, M.S. & ZOCCO, A. 2016 Viriato: A fourier–hermite spectral code for strongly magnetized fluid–kinetic plasma dynamics. *Computer Physics Communications* **206**, 45–63.
- MAJESKI, R., BELL, R. E., BOYLE, D. P., KAITA, R., KOZUB, T., LEBLANC, B. P., LUCIA, M., MAINGI, R., MERINO, E., RAITSES, Y., SCHMITT, J. C., ALLAIN, J. P., BEDOYA, F., BIALEK, J., BIEWER, T. M., CANIK, J. M., BUZI, L., KOEL, B. E., PATINO, M. I., CAPECE, A. M., HANSEN, C., JARBOE, T., KUBOTA, S., PEEBLES, W. A. & TRITZ, K. 2017 Compatibility of lithium plasma-facing surfaces with high edge temperatures in the Lithium Tokamak Experiment. *Physics of Plasmas* **24** (5), 056110, arXiv: https://pubs.aip.org/aip/pop/article-pdf/doi/10.1063/1.4977916/15997017/056110_1_online.pdf.
- MANDELL, N.R., DORLAND, W., ABEL, I., GAUR, R., KIM, P., MARTIN, M. & QIAN, T. 2022 GX: a GPU-native gyrokinetic turbulence code for tokamak and stellarator design. *arXiv preprint arXiv:2209.06731* .

- NAJMABADI, FARROKH, CONN, R.W. & COHEN, RONALD H. 1984 Collisional end loss of electrostatically confined particles in a magnetic mirror field. *Nuclear Fusion* **24** (1), 75.
- OCHS, IAN E., MUNIROV, VADIM R. & FISCH, NATHANIEL J. 2023 Confinement time and ambipolar potential in a relativistic mirror-confined plasma. *Physics of Plasmas* **30** (5).
- PARKER, JOSEPH T. & DELLAR, PAUL J. 2015 Fourier–hermite spectral representation for the vlasov–poisson system in the weakly collisional limit. *Journal of Plasma Physics* **81** (2), 305810203.
- PASTUKHOV, V.P. 1974 Collisional losses of electrons from an adiabatic trap in a plasma with a positive potential. *Nuclear Fusion* **14** (1), 3.
- PERRONE, L. M., JORGE, R. & RICCI, P. 2020 Four-dimensional drift-kinetic model for scrape-off layer plasmas. *Physics of Plasmas* **27** (11), 112502, arXiv: https://pubs.aip.org/aip/pop/article-pdf/doi/10.1063/5.0024968/16099478/112502_1_online.pdf.
- PEZZI, ORESTE, CAMPOREALE, ENRICO & VALENTINI, FRANCESCO 2016 Collisional effects on the numerical recurrence in Vlasov-Poisson simulations. *Physics of Plasmas* **23** (2), 022103, arXiv: https://pubs.aip.org/aip/pop/article-pdf/doi/10.1063/1.4940963/15794445/022103_1_online.pdf.
- POST, RICHARD F. & ROSENBLUTH, M.N. 1966 Electrostatic instabilities in finite mirror-confined plasmas. *The Physics of Fluids* **9** (4), 730–749.
- ROSENBLUTH, MARSHALL N., MACDONALD, WILLIAM M. & JUDD, DAVID L. 1957 Fokker-Planck equation for an inverse-square force. *Physical Review* **107** (1), 1.
- RYUTOV, D.D., BERK, H.L., COHEN, B.I., MOLVIK, A.W. & SIMONEN, T.C. 2011 Magneto-hydrodynamically stable axisymmetric mirrors. *Physics of Plasmas* **18** (9).
- SHARMA, PRATEEK & HAMMETT, GREGORY W 2011 A fast semi-implicit method for anisotropic diffusion. *Journal of Computational Physics* **230** (12), 4899–4909.
- TAITANO, WILLIAM T., CHACÓN, LUIS, SIMAKOV, A.N. & MOLVIG, K. 2015 A mass, momentum, and energy conserving, fully implicit, scalable algorithm for the multi-dimensional, multi-species Rosenbluth–Fokker–Planck equation. *Journal of Computational Physics* **297**, 357–380.
- ULBL, PHILIPP, BODY, THOMAS, ZHOLOBENKO, WLADIMIR, STEGMEIR, ANDREAS, PFENNIG, JAN & JENKO, FRANK 2023 Influence of collisions on the validation of global gyrokinetic simulations in the edge and scrape-off layer of tcv. *Physics of Plasmas* **30** (5).
- ULBL, PHILIPP, MICHELS, DOMINIK & JENKO, FRANK 2022 Implementation and verification of a conservative, multi-species, gyro-averaged, full-f, Lenard-Bernstein/Dougherty collision operator in the gyrokinetic code GENE-X. *Contributions to Plasma Physics* **62** (5-6), e202100180, arXiv: <https://onlinelibrary.wiley.com/doi/pdf/10.1002/ctpp.202100180>.
- WHITE, ROSCOE, HASSAM, ADIL & BRIZARD, ALAIN 2018 Centrifugal particle confinement in mirror geometry. *Physics of Plasmas* **25** (1).
- YE, BOYANG, HU, JINGWEI, SHU, CHI-WANG & ZHONG, XINGHUI 2024 Energy-conserving discontinuous galerkin methods for the vlasov-ampère system with dougherty-fokker-planck collision operator. *Journal of Computational Physics* **514**, 113219.

Appendix A. Convenient choice for the free function $q(\bar{v})$

We will prove equation (2.17) by first examining the delta function $\delta(1 - \mu^2)$ to transform it in terms of ρ . Recalling equation (2.14), we reorganize this definition to have equality

$$\frac{Z_s \mu^2 \rho^2}{4\bar{v}^4} e^{-2\bar{v}^2} = 1 - \mu^2. \quad (\text{A1})$$

Using the delta function to assert that $\mu = \pm 1$, we can show that the delta function transforms to

$$\delta(1 - \mu^2) = \delta\left(\frac{Z_s \rho^2}{4\bar{v}^4} e^{-2\bar{v}^2}\right) = \delta(\rho) \frac{2\bar{v}^4}{Z_s \rho} e^{2\bar{v}^2}, \quad (\text{A2})$$

where we have used $\delta(g(x)) = \delta(x - x_0)/|g'(x_0)|$ with x_0 satisfying $g(x_0) = 0$. Transforming $Q(\bar{v}, \mu)$, we then get

$$\frac{\pi^{3/2}}{2z \ln(z)} \frac{\delta(1 - \mu^2)}{4\pi} H(\bar{v} - a)q(\bar{v}) = \frac{\delta(\rho)}{2\pi\rho} H(z - z_a)4\pi \left(\frac{z \ln(z) \sqrt{\pi}}{8Z_s} q(\bar{v}) \right), \quad (\text{A } 3)$$

where we have grouped terms to get it in the form of equation (2.16). We find equation (2.17) by setting $q(\bar{v})$ to cancel out this functional dependence and leave within it some arbitrary functionality \bar{q} , which is set to a constant for simplicity.

Appendix B. Investigation into the correction factor in Najmabadi *et al.* (1984)

The notation used in this paper is very similar to the notation used in Najmabadi *et al.* (1984). For clarity, let us define some of the key differences in notation, which will be used exclusively in this appendix section. For the collision operator used in Najmabadi *et al.* (1984), they define the appropriate collision frequency and anisotropic diffusion coefficients considering multispecies collisions.

$$\nu_e \equiv \frac{4\pi}{m_e^2 v_{th,e}^3} \left(\frac{e^2}{4\pi\epsilon_0} \right)^2 n_e \lambda_{ee}, \quad Z_{e,N} \equiv \frac{1}{2} \left(1 + \frac{\sum_j n_j z_j^2 \lambda_{ej}}{n_e \lambda_{ee}} \right), \quad (\text{B } 1)$$

$$\nu_i \equiv 4\pi \left(\frac{e^2}{4\pi\epsilon_0} \right)^2 \sum_j \frac{n_j z_i^2 z_j^2 \lambda_{ij}}{m_i m_j v_{th,i}^2 T_i}, \quad Z_{i,N} \equiv \frac{1}{2} \frac{\sum_j n_j z_j^2 \lambda_{ij}}{\sum_j n_j z_j^2 \lambda_{ij} (T_j/T_i) (m_i/m_j)}. \quad (\text{B } 2)$$

where \sum_j is a summation over ions only, $v_{th,s} = \sqrt{2T_s/m_s}$ e is the electronic charge, z_s is the atomic number of species s , λ_{ab} is the Coulomb logarithm, and ϵ_0 is the dielectric constant.

We restate the main finding from Najmabadi *et al.* (1984). They found that the confinement time scales as

$$\frac{1}{\tau_{c,N}} = \nu_s \frac{4}{\sqrt{\pi}} \frac{\exp(-a^2) (Z_{s,N} + 1/4) a^2 \exp(a^2) E_1(a^2) - 1/4}{a^2 \ln\left(\frac{w+1}{w-1}\right) - c_N}. \quad (\text{B } 3)$$

Here, $w = \sqrt{1 + 2/(R(Z_s - T_s/4z_s e\phi))}$, and $a^2 = z_s e\phi/T_s + \ln(w)$, $E_1(x) = \int_x^\infty dt \exp(-t)/t$ is the exponential integral, c_N is a correction coefficient, and the subscript N stands for Najmabadi *et al.* (1984),[†]. In Najmabadi *et al.* (1984), they determine $c_N = 0.84$, although we have not replicated the calculation used to determine c_N . Instead, we opt to apply the same numerical technique employed in section 3. By calculating the value of c_N that minimizes the error between our finite element model, we determine the appropriate value of c_N . Table 2 has the appropriate correction coefficients for a pure hydrogen plasma ($Z_s = 1/2$), and table 3 has the correction coefficients for electrons with a hydrogen background ($Z_s = 1$). Intriguingly, this coefficient depends on the pitch angle scattering rate Z_s . It is clear from these tables that Najmabadi *et al.* (1984) calculated this as a constant, but it has a much more complicated dependency in matching the finite element model. It is essential to mention that the collision operator utilized by the finite element model is approximate, especially at low velocities, which impacts the results at low values of $z_s e\phi/T_s$. However, it is intriguing that this coefficient does not asymptote to a constant at large values of R or $z_s e\phi/T_s$, which they

[†] There is a typo in the second statement of w in Najmabadi *et al.* (1984) near equation (42) which should have a square root, noticed by Ochs *et al.* (2023).

$z_s e\phi/T_s$	R									
	5	10	15	20	25	30	35	40	45	50
1	0.876	0.860	0.777	0.770	0.691	0.702	0.680	0.653	0.649	0.679
2	1.056	1.030	1.009	0.967	0.965	0.965	0.942	0.940	0.928	0.924
3	1.095	1.082	1.062	1.046	1.034	1.021	1.016	1.008	0.996	1.017
4	1.114	1.107	1.091	1.078	1.067	1.058	1.051	1.044	1.039	1.035
5	1.126	1.121	1.106	1.093	1.083	1.075	1.068	1.062	1.057	1.053
6	1.134	1.131	1.117	1.104	1.095	1.087	1.080	1.075	1.070	1.064
7	1.136	1.132	1.117	1.104	1.095	1.086	1.080	1.073	1.068	1.066
8	1.138	1.133	1.119	1.106	1.098	1.089	1.081	1.076	1.070	1.068
9	1.142	1.140	1.127	1.117	1.103	1.095	1.088	1.085	1.083	1.079
10	1.142	1.141	1.123	1.118	1.106	1.093	1.084	1.079	1.079	1.091

TABLE 2. A table of optimal correction factors c_N for various values of $z_s e\phi/T_s$ and R to minimize error with the finite element model for ions $Z_s = 1/2$.

$z_s e\phi/T_s$	R									
	5	10	15	20	25	30	35	40	45	50
1	1.183	1.125	1.093	1.068	1.052	1.040	1.031	1.023	1.017	1.013
2	1.093	1.046	1.018	0.999	0.986	0.976	0.968	0.963	0.958	0.953
3	1.081	1.042	1.018	1.002	0.991	0.983	0.976	0.971	0.966	0.963
4	1.090	1.056	1.035	1.020	1.010	1.003	0.997	0.992	0.988	0.984
5	1.101	1.069	1.048	1.034	1.026	1.018	1.012	1.008	1.004	1.001
6	1.112	1.083	1.062	1.048	1.041	1.033	1.028	1.023	1.020	1.014
7	1.115	1.084	1.063	1.049	1.042	1.035	1.029	1.024	1.020	1.020
8	1.119	1.088	1.067	1.054	1.046	1.038	1.033	1.030	1.024	1.023
9	1.127	1.097	1.078	1.066	1.054	1.050	1.043	1.042	1.041	1.035
10	1.124	1.096	1.075	1.071	1.056	1.052	1.035	1.032	1.044	1.033

TABLE 3. A table of optimal correction factors c_N for various values of $z_s e\phi/T_s$ and R to minimize error with the finite element model for pure electrons $Z_s = 1$.

suggest should. Furthermore, utilizing this coefficient table effectively provides a much better estimation of the results from the finite element model than the original work. Nonetheless, all figures in the rest of the paper are produced with $c_N = 0.84$ as it still is a reasonable estimate.

Appendix C. Loss cone boundary conditions

From equations (2.3), we have two boundary conditions to fix q_0 and a . Recall $g(\bar{v}, \mu) = \pi^{3/2} \exp(\bar{v}^2) F_s(\bar{v}, \mu)$, and hence

$$g(\rho, z)|_{z=z_0, \rho=0} = 0. \quad (\text{C1})$$

This is straightforward to apply from equation (2.19),

$$q_0 = \left(\ln \left(\frac{w+1}{w-1} \right) \right)^{-1}, \quad (\text{C2})$$

where $w = \exp(a^2 - \bar{v}_0^2)$. Equation (C2) can be rewritten as $w = \coth(1/2q_0)$.

Now, we will expand the second condition in equation (2.3), that the curvature of the

contour where our fitted distribution function is zero near the loss cone matches the curvature of the true loss cone. For the sake of generality, we will refer to a variable transformation where the velocity transformation is the same, $z = \exp(\bar{v}^2)$, but the pitch angle transformation is in the general form of $\rho = \bar{\rho}(\bar{v})z\sqrt{1-\mu^2}/\mu = \bar{\rho}(\bar{v})z \tan \theta \approx \bar{\rho}(\bar{v})z\theta$ where we have isolated the separate pitch angle and velocity dependence. With this form,

$$\partial_{\bar{v}}F(\bar{v}, \mu) = \partial_{\bar{v}} \left(\frac{g(\rho, z)}{\pi^{3/2}z} \right) = \frac{1}{\pi^{3/2}z} \partial_{\bar{v}}g(\rho, z), \quad (\text{C3})$$

and

$$\partial_{\mu}F(\bar{v}, \mu) = \partial_{\mu} \left(\frac{g(\rho, z)}{\pi^{3/2}z} \right) = \frac{1}{\pi^{3/2}z} \partial_{\mu}g(\rho, z). \quad (\text{C4})$$

So from changing distribution function from $F_s(\bar{v}, \mu)$ to $g(\rho, z)$,

$$\left. \frac{\partial_{\bar{v}}g}{\partial_{\mu}g} \right|_{z=z_0, \rho=0} = \frac{1}{R\bar{v}_0}, \quad (\text{C5})$$

where we have used $g(0, z_0) = 0$. Continuing, we must expand the partial derivatives in \bar{v} and μ into their respective derivatives in terms of ρ and z using the chain rule,

$$\partial_{\bar{v}}g(\rho, z) = \frac{\partial g}{\partial \rho} \frac{\partial \rho}{\partial \bar{v}} + \frac{\partial g}{\partial z} \frac{\partial z}{\partial \bar{v}} = \frac{\partial g}{\partial \rho} \rho \left(2\bar{v} + \frac{\bar{\rho}'}{\bar{\rho}} \right) + \frac{\partial g}{\partial z} 2\bar{v}z, \quad (\text{C6})$$

$$\partial_{\mu}g = \frac{\partial g}{\partial \rho} \frac{\partial \rho}{\partial \mu} = \frac{\partial g}{\partial \rho} \frac{\partial \rho}{\partial(\cos \theta)} \approx \frac{\partial g}{\partial \rho} \frac{\partial \rho}{-\theta \partial \theta} = \frac{\partial g}{\partial \rho} \frac{\bar{\rho}(\bar{v})z}{-\theta} = -\frac{\partial g}{\partial \rho} \frac{\rho}{\theta^2}. \quad (\text{C7})$$

One of the beautiful aspects of this derivation is that this specific choice of variables results in a simple form of the derivative in μ . Furthermore, it can be shown that the derivatives of equation (2.19) are

$$\left. \frac{\partial g}{\partial z} \right|_{z=z_0, \rho=0} = -\frac{2q_0w}{z_0(w^2-1)}, \quad (\text{C8})$$

$$\left. \frac{\partial g}{\partial \rho} \right|_{z=z_0, \rho \ll 1} = -\frac{q_0\rho}{2z_0^2} \left[\frac{1}{(w+1)^2} - \frac{1}{(w-1)^2} \right]. \quad (\text{C9})$$

Now we can plug it all back in together,

$$\frac{1}{R\bar{v}_0} = \frac{\frac{\partial g}{\partial \rho} \rho \left(2\bar{v} + \frac{\bar{\rho}'}{\bar{\rho}} \right) + \frac{\partial g}{\partial z} 2\bar{v}z}{\frac{q_0}{2z_0^2} \left[\frac{1}{(w+1)^2} - \frac{1}{(w-1)^2} \right] \frac{\rho^2}{\theta^2}} \Bigg|_{z=z_0, \rho \rightarrow 0}. \quad (\text{C10})$$

Next, we notice that $\rho \rightarrow 0$ and $\partial_{\rho}g \propto \rho$, so the $\partial_{\rho}g$ term in the numerator is negligible. We also see that $\rho^2/\theta^2 = \bar{\rho}^2 z_0^2$ for $z = z_0$ and $\theta \ll 1$, giving

$$\frac{1}{R\bar{v}_0} = \frac{2\bar{v}_0}{\bar{\rho}(\bar{v}_0)^2} (w^2 - 1). \quad (\text{C11})$$

Solving for w we find equation (2.21). For the collision operator in Najmabadi *et al.* (1984), $\bar{\rho}(\bar{v})^2 = 2\bar{v}^2/(Z_s - 1/4\bar{v}^2)$, so their equivalent expression would be

$$w^2 = 1 + \frac{1}{R(Z_s - 1/4\bar{v}_0^2)}, \quad (\text{C12})$$

which agrees with the results of Najmabadi *et al.* (1984). For Dougherty, we use $\bar{\rho}(\bar{v})^2 = 4\bar{v}^4/Z_s$ so the matching condition becomes the second equality in equation (2.21).